JPET Fast Forward. Published on August 3, 2023 as DOI: 10.1124/jpet.123.001591
This article has not been copyedited and formatted. The final version may differ from this version.

# TITLE PAGE

## Mechanistic Model Describing the Time Course of Humoral Immunity Following Ad26.COV2.S Vaccination in Non-Human Primates*

Anna Dari[1], Laura Solforosi[2], Ramon Roozendaal[2], Richard M.W. Hoetelmans[1], Juan-José Pérez-Ruixo[1], Muriel Boulton[1]

[1]Janssen Research and Development, Beerse, Belgium; [2]Janssen Vaccines and Prevention B.V., Leiden, The Netherlands

JPET Fast Forward. Published on August 3, 2023 as DOI: 10.1124/jpet.123.001591
This article has not been copyedited and formatted. The final version may differ from this version.

# RUNNING TITLE PAGE

**Running title:** Mechanistic Modeling of Humoral Immunity in NHPs

**Corresponding author**: Anna Dari, Janssen Research and Development, Turnhoutseweg 30, 2340 Beerse, Antwerp, Belgium; adari1@its.jnj.com

The number of text pages: 35

The number of tables: 3

The number of figures: 5

The number of references: 40

The number of words in the Abstract: 240

The number of words in Introduction: 722

The number of words in Discussion: 1493

A list of nonstandard abbreviations used in the paper (alphabetical order):

Ad26, adenovirus serotype 26

CoP, correlate of protection

COVID-19, coronavirus disease 2019

CWRES, conditional weighted residuals

GC, germinal center

IIV, inter-individual variability

MIM, minimal immunogenicity response marker

MVOF, minimum value objective function

NHP, non-human primate

S, spike

SARS-CoV-2, severe acute respiratory syndrome coronavirus 2

S-ELISA, spike protein–enzyme-linked immunosorbent assay

vp, viral particles

VPC, visual predictive check

JPET Fast Forward. Published on August 3, 2023 as DOI: 10.1124/jpet.123.001591
This article has not been copyedited and formatted. The final version may differ from this version.

A recommended section assignment to guide the listing in the table of contents:

Drug Discovery and Translational Medicine

JPET Fast Forward. Published on August 3, 2023 as DOI: 10.1124/jpet.123.001591
This article has not been copyedited and formatted. The final version may differ from this version.

## ABSTRACT

Mechanistic modeling can be used to describe the time course of vaccine-induced humoral immunity and to identify key biological drivers in antibody production. We utilized a six-compartment mechanistic model to describe a 20-week time course of humoral immune responses in 56 non-human primates (NHPs) elicited by vaccination with Ad26.COV2.S according to either a single-dose regimen ($1 \times 10^{11}$ or $5 \times 10^{10}$ viral particles [vp]) or a two-dose homologous regimen ($5 \times 10^{10}$ vp) given in an interval of 4 or 8 weeks. Humoral immune responses were quantified by severe acute respiratory syndrome coronavirus 2 (SARS-CoV-2) spike–specific binding antibody concentrations as determined by spike protein–enzyme-linked immunosorbent assay (S-ELISA). The mechanistic model adequately described the central tendency and variability of binding antibody concentrations through 20 weeks in all vaccination arms. The estimation of mechanistic modeling parameters revealed greater contribution of the antibody production mediated by short-lived cells as compared to long-lived cells in driving the peak response, especially post second dose when a more rapid peak response was observed. The antibody production mediated by long-lived cells was identified as relevant for generating the first peak and for contributing to the long-term time course of sustained antibody concentrations in all vaccination arms. The findings contribute evidence on the key biological components responsible for the observed time course of vaccine-induced humoral immunity in NHPs and constitute a step toward defining immune biomarkers of protection against SARS-CoV-2 that might translate across species.

JPET Fast Forward. Published on August 3, 2023 as DOI: 10.1124/jpet.123.001591
This article has not been copyedited and formatted. The final version may differ from this version.

## SIGNIFICANCE STATEMENT

We demonstrate the adequacy of a mechanistic modeling approach describing the time course of binding antibody concentrations in non-human primates (NHPs) elicited by different dose levels and regimens of Ad26.COV2.S. The findings are relevant for informing the mechanism-based accounts of vaccine-induced humoral immunity in NHPs and translational research efforts aimed at identifying immune biomarkers of protection against SARS-CoV-2 infection.

JPET Fast Forward. Published on August 3, 2023 as DOI: 10.1124/jpet.123.001591
This article has not been copyedited and formatted. The final version may differ from this version.

## INTRODUCTION

Deployment of vaccines has been instrumental in controlling the pandemic of coronavirus disease 2019 (COVID-19) caused by severe acute respiratory syndrome coronavirus 2 (SARS-CoV-2) (Machado et al., 2022). Several vaccines have been shown to induce humoral immune responses to SARS-CoV-2 and have proven effective in protecting against COVID-19 trial endpoints (Goldblatt et al., 2022; Gruell et al., 2022).

Janssen's COVID-19 vaccine, Ad26.COV2.S, is an adenovirus serotype 26 (Ad26) vector-based vaccine encoding a full-length, prefusion-stabilized SARS-CoV-2 spike (S) protein (Bos et al., 2020; Sadoff et al., 2021b). When administered at a dose of $5 \times 10^{10}$ or $1 \times 10^{11}$ viral particles (vp), Ad26.COV2.S elicited S protein–binding and neutralizing antibody responses in >88% of participants at day 29 post vaccination in a clinical phase 1–2a trial (Sadoff et al., 2021b). In the subsequent analysis of phase 1–2a data, durable binding and neutralizing antibody responses were observed for 6 to 8 months following vaccination with single-dose Ad26.COV2.S ($5 \times 10^{10}$ vp), and were robustly increased following homologous boosting at 2 and 6 months (Sadoff et al., 2022b).

The efficacy of single-dose and booster regimens of Ad26.COV2.S was evaluated in the subsequent phase 3, double-blind, placebo-controlled, randomized trials (Sadoff et al., 2021a; Hardt et al., 2022; Sadoff et al., 2022a). Vaccine efficacy of single-dose Ad26.COV2.S ($5 \times 10^{10}$ vp) for the prevention of molecularly confirmed, moderate to severe–critical COVID-19 was reported to be 56.3% and 52.9%, with onset ≥14 days and ≥28 days following vaccination, respectively (ENSEMBLE) (Sadoff et al., 2022a). In the ENSEMBLE2 trial, a primary dose of Ad26.COV2.S ($5 \times 10^{10}$ vp) followed by a homologous booster at 2 months had an efficacy of 75.2% against molecularly confirmed, moderate to severe–critical COVID-19 with onset ≥14 days after boosting (Hardt et al., 2022).

JPET Fast Forward. Published on August 3, 2023 as DOI: 10.1124/jpet.123.001591
This article has not been copyedited and formatted. The final version may differ from this version.

Due to increasing challenges in evaluating the long-term efficacy of COVID-19 vaccines in a placebo-controlled trial setting (Roozendaal et al., 2021; Goldblatt et al., 2022), establishing immune biomarkers that correlate with protection (i.e., correlates of protection [CoP]) could accelerate approval of modified regimens of existing vaccines (Koup et al., 2021) and facilitate estimating the durability of vaccine-induced protection (Sherman et al., 2022). Defining CoP against COVID-19 endpoints, however, requires substantial phase 3 trial evidence generated in different populations, vaccine platforms, and viral variants (Koup et al., 2021).

The use of non-human primate (NHP) models has been vital for informing the translational application of COVID-19 vaccines (Qi and Qin, 2022), and has contributed valuable data on humoral CoP following vaccination with Ad26.COV2.S (Mercado et al., 2020; McMahan et al., 2021; Roozendaal et al., 2021). In NHP models, the protective efficacy of Ad26.COV2.S has been defined in relation to the reduction of viral replication (associated with virus extinction instead of viral growth) in different anatomic compartments (i.e., upper and lower airways) (Roozendaal et al., 2021). Using a mechanistic modeling approach, we recently observed that increasing concentrations of S protein–binding antibody at week 4 post immunization with single-dose Ad26.COV2.S were associated with increasing protective efficacy in the lung and the nose of vaccinated animals (Roozendaal et al., 2021). In addition, the protection against SARS-CoV-2 in a NHP challenge model correlated with immune biomarker levels used in the study (binding and neutralizing antibody) elicited by different doses of Ad26.COV2.S (He et al., 2022). By extension, vaccine-induced circulating binding and neutralizing antibodies in humans correlated with vaccine efficacy against COVID-19 endpoints up to 4 months post immunization with single-dose Ad26.COV2.S vaccine (Fong et al., 2022) and double-dose mRNA-1273 vaccine (Gilbert et al., 2022).

JPET Fast Forward. Published on August 3, 2023 as DOI: 10.1124/jpet.123.001591
This article has not been copyedited and formatted. The final version may differ from this version.

We have recently demonstrated the adequacy of a six-compartment mechanistic model for describing the time course of humoral immune responses in humans through 8 months following single-dose ($5 \times 10^{10}$ vp) vaccination with Ad26.COV2.S (Dari et al., 2022). These findings raise a question about the suitability of the mechanistic modeling approach to characterize the time course of humoral immune responses elicited by different dose levels and regimens of Ad26.COV2.S in humans and animal species. The objective of this study was to describe the time course of humoral immune responses in NHPs elicited by multiple vaccination regimens of Ad26.COV2.S including single-dose regimens administered at dose levels of $1 \times 10^{11}$ and $5 \times 10^{10}$ vp and two-dose homologous regimens administered at a dose level of $5 \times 10^{10}$ vp given at an interval of 4 or 8 weeks.

## METHODS

### Study Design

Two study arms involved administration of single-dose Ad26.COV2.S ($1 \times 10^{11}$ or $5 \times 10^{10}$ vp), and two study arms involved administration of two doses of $5 \times 10^{10}$ vp given either 4 or 8 weeks apart (Table 1) (Solforosi et al., 2021). Humoral immune response data were collected up to 20 weeks in 56 NHPs (adult rhesus macaques; 53 females and 3 males, 3.3-5.1 yr old, 2.9-7.2 kg) assigned to one of these four vaccination arms (Solforosi et al., 2021; Solforosi et al., 2022). Blood samples for measuring humoral immune responses were collected before first immunization (day 1, baseline) and on days 15, 29, 43, 57, 71, 86, 99, 113, 127, and 141 post first immunization; on day 141, only samples from 7 NHPs per arm were collected and analyzed. Humoral immune responses were measured using the validated S protein–enzyme-linked immunosorbent assay (S-ELISA). Baseline values were not considered in the analysis, although S-ELISA values above the lower limit of quantification ([LLOQ], 50.3 $\log_{10}$ EU/mL) were reported in 1 NHP. Animal experiment was approved by

JPET Fast Forward. Published on August 3, 2023 as DOI: 10.1124/jpet.123.001591
This article has not been copyedited and formatted. The final version may differ from this version.

the Institutional Animal Care and Use Committee at Charles River Laboratories Montreal ULC, Laval Site (CA).

**Immunogenicity Assay**

*S-ELISA*

ELISA was developed and qualified for human serum at Nexelis, Laval, Canada. In brief, purified SARS-CoV-2 spike antigen was adsorbed to the wells of a microplate, and diluted serum samples (test samples, standard, and quality controls) were added. Unbound sample was washed away, followed by incubation with an enzyme-conjugated anti-human IgG and colorimetric detection with tetramethylbenzidine. A reference standard on each test plate was used to quantify the amount of antibodies against SARS-CoV-2 spike in the sample according to the unit assigned by the standard (EU/mL). The S-ELISA assay was described previously (Solforosi et al., 2021).

**Structural Model**

The structural model considered the key elements of humoral immune response (Wilson et al., 2007; Pasin et al., 2019; Balelli et al., 2020; Dari et al., 2022): the antigen (Ag, S protein), the B cells (M), the short-lived cells (S), the long-lived cells (L), the antibody in serum (Ab), and the antibody in peripheral sites (P) (Fig. 1).

The relationship between vaccine dosing and antigen effects on antibody response was described through a virtual antigen compartment from a kinetics of drug action model (Jacqmin et al., 2007), as described by Equation 1:

$$\frac{dAg}{dt} = -k_{Ag} \cdot Ag - k_{on} \cdot Ag \cdot Ab \qquad \text{Equation 1}$$

where $k_{Ag}$ is the first-order equilibration rate constant quantifying the apparent non-specific decay of S protein (Balelli et al., 2020), $k_{on}$ is the second-order constant quantifying the

JPET Fast Forward. Published on August 3, 2023 as DOI: 10.1124/jpet.123.001591
This article has not been copyedited and formatted. The final version may differ from this version.

elimination of the antigen (S protein) due to binding to the antibody against S protein (Schley et al., 2012; Zarnitsyna et al., 2015; Bonin et al., 2018), consistent with antibody feedback hypothesis whereby higher-affinity antibodies produced by germinal center (GC)–derived plasma cells re-enter GC and restrict antigen access over time (Zhang et al., 2013).

The time course of B cell responses was described using two proliferation terms to capture differential dynamics of B cell responses as generated directly by the memory B cell formation ($M_1$) and GC pathway ($M_2$) (on the assumption that GC and memory B cells are dominant cell populations within more complex dynamics). Immunization is assumed to induce the production of short-lived cells over time through the memory B cell pathway (Zhang et al., 2013; McNamara et al., 2020). This might be especially relevant for explaining the faster peak response that was observed post second dose of Ad26.COV2.S. By contrast, long-lived cells are assumed to be predominantly produced through GC (Zhang et al., 2013; McNamara et al., 2020), and might be especially relevant for explaining the slower peak response post first dose as well as long-term time course of sustained antibody concentrations in all vaccination arms. The features of B cell dynamics are described by Equations 2 and 3:

$$\frac{dM_1}{dt} = \left(k_{pAg} \cdot Ag + k_{pM} \cdot M_1\right)\left(1 - \frac{M_1}{N_1}\right) - \left[k_{pS} \cdot Ag + k_{eM_1}\right] \cdot M_1 \qquad \text{Equation 2}$$

$$\frac{dM_2}{dt} = \left(k_{pAg} \cdot Ag\right) - \left[k_{pL} \cdot Ag + k_{eM_2}\right] \cdot M_2 \qquad \text{Equation 3}$$

where $k_{pAg}$ is the first-order rate constant of antigen-dependent B cell differentiation into short-lived and long-lived cells through the memory B cell formation ($M_1$) and GC ($M_2$) pathways, respectively. The term $k_{pM}$ denotes the production rate of memory B cells through an antigen-independent pathway which quickly reaches a maximum cell growth level ($N_1$).

The $k_{pS}$ and $k_{pL}$ denote differentiation rates of B cells into short-lived and long-lived cells, respectively (Inoue et al., 2018; Balelli et al., 2020) which are also stimulated by antigen

JPET Fast Forward. Published on August 3, 2023 as DOI: 10.1124/jpet.123.001591
This article has not been copyedited and formatted. The final version may differ from this version.

presence; $k_{eM_1}$ and $k_{eM_2}$ are the first-order rate constants of the antigen-independent elimination of B cells through $M_1$ and $M_2$, respectively.

The production of short-lived and long-lived cells is assumed to be a second-order process, contingent on the amount of antigen and the available B cells (Dari et al., 2022):

$$\frac{dS}{dt} = k_{pS} \cdot Ag \cdot M_1 - k_{eS} \cdot S \quad \text{Equation 4}$$

$$\frac{dL}{dt} = k_{pL} \cdot Ag \cdot M_2 - k_{eL} \cdot L \quad \text{Equation 5}$$

where $k_{eS}$ and $k_{eL}$ denote the first-order elimination rate constants of short-lived and long-lived cells, respectively. The assumed half-life of short-lived cells is in the range of days, while the long-lived cells are assumed to persist and maintain serum antibody levels for years in the absence of memory B cells (Hammarlund et al., 2017; Inoue et al., 2018; Nguyen et al., 2021).

We assumed proportionality between the serum antibody production and the amount of short-lived and long-lived cells, and characterized antibody disposition (distribution and elimination) by the first-order elimination and linear distribution to a non-specific peripheral compartment as described by Equations 6 and 7:

$$\frac{dAb}{dt} = k_{AbS} \cdot S + k_{AbL} \cdot L - k_{eAb} \cdot Ab - k_{AbP} \cdot Ab + k_{PAb} \cdot P \quad \text{Equation 6}$$

$$\frac{dP}{dt} = k_{AbP} \cdot Ab - k_{PAb} \cdot P \quad \text{Equation 7}$$

where $k_{AbS}$ and $k_{AbL}$ represent the first-order production rate constants of antibodies from short-lived and long-lived cells, respectively; $k_{AbP}$ denotes the non-specific distribution to a peripheral compartment, $k_{PAb}$ denotes the return of antibodies from the peripheral compartment to the serum compartment, and $k_{eAb}$ denotes a first-order elimination rate constant of the serum antibodies.

JPET Fast Forward. Published on August 3, 2023 as DOI: 10.1124/jpet.123.001591
This article has not been copyedited and formatted. The final version may differ from this version.

It was assumed that the antibodies were produced well in excess relative to the amount of antigen, such that the amount of antigen was negligible relative to the amount of antibody. By this assumption, the antibody disposition was not affected by the binding to the antigen and can be regarded as similar to the disposition of monoclonal antibodies after intravenous administration that did not exhibit target-mediated drug disposition. This assumption also implies the elimination of the antigen (S protein) due to binding to the antibody against S protein as described by Equation 1.

**Model Parameters**

The following parameters were estimated: $k_{AbS}$, $k_{AbL}$, $k_{eS}$, $k_{pM}$, $k_{on}$, and the maximum B cell growth in the memory B cell formation pathway ($N_1$). Because only binding antibody data were available at the time of the analysis, several parameters were fixed based on literature or tested through sensitivity analysis, as detailed below and in the Supplementary Materials (Section 1.3).

The elimination rate constants of long-lived plasma cells ($k_{eL}$), and of the B cells through $M_1$ and $M_2$ ($k_{eM1}$, $k_{eM2}$) were set to zero due to the time frame of the collected data (20 weeks), which is shorter than the respective half-life reported in the literature (several years) (Pasin et al., 2019; Balelli et al., 2020; He et al. 2022). The parameters characterizing antibody disposition were derived from the study reporting the disposition of antibodies with linear pharmacokinetics in humans (Davda et al., 2014) and were adjusted to NHP values via allometric scaling considering the mean body weight of 4.5 kg of the NHPs enrolled in this study. The allometric exponents equaled to 0.75 for clearance, and 1 for volume (Dong et al., 2011). The scaled antibody disposition parameters for NHPs were clearance from the central compartment of 0.026 L/day, volume from the central compartment of 0.23 L, inter-compartmental distribution clearance of 0.095 L/day, and volume of peripheral compartment

JPET Fast Forward. Published on August 3, 2023 as DOI: 10.1124/jpet.123.001591
This article has not been copyedited and formatted. The final version may differ from this version.

of 0.177 L. The micro rates ($day^{-1}$) were derived as $k_{eAb}$ of 0.11, $k_{AbP}$ of 0.41, and $k_{PAb}$ of 0.54. The terminal elimination half-life of the antibody in NHPs was computed at 11.7 days considering the beta phase of the two-compartment model after intravenous administration.

Inter-individual variability (IIV) could be estimated on $k_{AbS}$, $k_{AbL}$, $k_{pM}$, and $k_{eS}$. The residual unexplained variability was characterized using an additive error model after logarithmic transformation of the predicted and measured antibody concentrations. Modeling analysis was conducted using the non-linear mixed-effect modeling software NONMEM® 7.4.3 (ICON plc, Hanover, MD, USA). Additional details on the IIV and residual variability models, and computer software are provided in the Supplementary Materials (Sections 1.1, 1.2 and 1.4, respectively).

**Model Evaluation**

A series of structural models were fitted to the data, and model selection was guided by assessing the improvement in the model fit through the likelihood ratio test ($P < 0.01$), which is based on the change in the minimum value of the objective function (MVOF) (Savic and Karlsson, 2009; Nguyen et al., 2017). In addition, models were evaluated by assessing the reduction in IIV/residual variability and the correlations between parameter estimates, as well as by examining diagnostic plots (goodness-of-fit plots), a visual predictive check (VPC) (Bergstrand et al., 2011), shrinkage, and precision of parameter estimates.

The VPC was performed by computing the mean and model-based 80% prediction interval from 1000 Monte Carlo replicates by using the resulting final model parameters. Based on the sampling schedule, the geometric mean of the model-based predictions was calculated and overlaid with the observed binding antibody concentrations. VPC plots were stratified by the vaccination arm and individual observations were added to the graph.

JPET Fast Forward. Published on August 3, 2023 as DOI: 10.1124/jpet.123.001591
This article has not been copyedited and formatted. The final version may differ from this version.

Deterministic simulations were performed, based on the parameter estimates of the mechanistic structural model and without incorporating any source of variations, to show the antibody time course of interpolated two-dose regimens, where the second dose of Ad26.COV2.S ($5 \times 10^{10}$ vp) was administered at 2-, 4-, 6-, and 8-week intervals following primary vaccination.

## RESULTS

### Data Exploration

As shown in Fig. 2A, vaccination with a single dose or two doses of Ad26.COV2.S induced sustained, detectable concentrations of binding antibody through 20 weeks in all vaccination arms. Serum binding antibody concentrations increased until peaking within 4 weeks following primary vaccination, and within 2 weeks following the second dose. Binding antibody concentrations subsequently showed a bi-exponential decline in all vaccination arms. When normalized by dose, binding antibodies had similar concentrations following single-dose injection of Ad26.COV2.S administered at $1 \times 10^{11}$ vp and $5 \times 10^{10}$ vp (Fig. 2B), consistent with the assumption associated with Equation 1.

Antibody concentrations (EU/mL $\log_{10}$) at the time of the second peak were comparable between the 4-week, two-dose regimen (day 43; median, 3.81; Q1=3.63, Q3=3.82) and the 8-week, two-dose regimen (day 71; median, 3.80; Q1=3.70, Q3=3.98) (Table 2). At the end of the observation period (day 141), the lowest antibody concentration was observed in the single-dose regimen of $5 \times 10^{10}$ vp Ad26.COV2.S (median, 2.56; Q1=2.39, Q3=2.73) (Table 2).

### Structural Model

JPET Fast Forward. Published on August 3, 2023 as DOI: 10.1124/jpet.123.001591
This article has not been copyedited and formatted. The final version may differ from this version.

The parameter estimates of the structural model are summarized in Table 3. All parameters were estimated with relative standard error of <22% for fixed effect and <14% for random effect. The shrinkage of random effects, ≤19%, was considered acceptable.

Among the six estimated parameters, the antigen-independent proliferation rate constant of $M_1$, $k_{pM}$, was 0.183 $day^{-1}$, and represented the rate of accumulation needed to reach a saturation value of $5.0 \cdot 10^5$ B cells starting from 6 weeks after first vaccination. These results are consistent with similar observed binding antibody concentrations of the second peak of both two-dose regimens, with the larger waning of antibody concentrations observed after the second peak compared to the first peak. The model that included $k_{on}$ as an estimated parameter resulted in significantly improved model fit (ΔMVOF=139, df=1; $P < 0.001$) as compared to the model where $k_{on}$ was fixed to 0, which could not successfully converge. The estimated $k_{on}$ was 1.15 (0.92 to 1.38) $\cdot 10^4$ $day^{-1}$/(EU/mL).

The estimated short-lived cell elimination rate, $k_{eS}$, was 0.30 (0.21 to 0.40) $day^{-1}$, resulting in a half-life duration of a few days, consistent with limited life-span of short-lived cells described in the literature (Nguyen et al., 2021). The estimated rates of antibody production by short-lived cells ($k_{AbS}$) and long-lived cells ($k_{AbL}$) were 2.37 and 0.582 $day^{-1}$ · (EU/mL)/Cells, respectively. The differences in the underlying dynamics of the $M_1$ and $M_2$ pathways and the similar fixed values chosen for $k_{pS}$ and $k_{pL}$ preclude an absolute comparison between $k_{AbS}$ and $k_{AbL}$. However, the estimated parameter values of $k_{AbS}$ and $k_{AbL}$ suggest a relatively larger contribution of the short-lived cells compared to long-lived cells in driving peak antibody production.

Goodness-of-fit plots indicate that the structural model adequately described the serum antibody concentration data (Fig. 3). The observations against the population and individual model predictions show a normal random scatter around the identity line (Fig. 3A). Similarly,

JPET Fast Forward. Published on August 3, 2023 as DOI: 10.1124/jpet.123.001591
This article has not been copyedited and formatted. The final version may differ from this version.

the plots of distribution of conditional weighted residuals (CWRES) vs. population predictions and time show the absence of systematic trends over the range of evaluated antibody concentrations and time points (Fig. 3B).

The correlation between the IIV random effects was relatively low with a maximum $r^2$= 0.18 between $k_{pM}$ and $k_{Ag}$. As evidenced by the VPC, the structural model adequately captured the time course of geometric mean serum concentrations induced by Ad26.COV2.S and their associated variability across all vaccination arms (Fig. 4).

Deterministic simulations showed that two-dose regimens of Ad26.COV2.S ($5 \times 10^{10}$ vp) were associated with a higher peak response compared to single-dose regimen ($5 \times 10^{10}$ vp) (Fig. 5). In agreement with observations from data exploration, the timing of administering the second dose between 4 and 8 weeks appeared less relevant as simulated data reached similar levels, especially for follow-up visits. At week 20, serum antibody concentrations following two-dose regimens were predicted to be at least 1.1–fold higher than the serum antibody concentrations post single dose. However, in both cases, the serum antibody concentrations were above the minimal concentration required for protection against replication of SARS-CoV-2 (quantified as the minimal concentration needed to bring the basic reproductive ratio of SARS-CoV-2 below 1). The minimal immunogenicity response marker [MIM] in the lung was 1.85 (95% CI, 1.80 to 1.91) EU/mL $\log_{10}$, which is lower than the MIM in the nose 3.21 (95% CI, 2.85 to 3.81) EU/mL $\log_{10}$ (data on file). This difference is mainly due to the lower basic reproductive ratio in lung than in nose (Gonçalves et al. 2021).

## DISCUSSION

JPET Fast Forward. Published on August 3, 2023 as DOI: 10.1124/jpet.123.001591
This article has not been copyedited and formatted. The final version may differ from this version.

The objective of the study was to describe the observed time course of serum binding antibody concentrations elicited by the administration of single-dose and two-dose regimens of Ad26.COV2.S in NHPs, as previously done in humans (Dari et al., 2022), via a mechanistic humoral immune response model. The comparison of model parameters between NHP and human was interpreted from a qualitative, rather than quantitative, point of view. The immune response was adequately described by the mechanistic model that considered the biphasic production and disposition of antibodies. The half-life of serum antibodies in NHPs between week 14 and 20 was 2.90 years, which is substantially longer than the computed value of 11.7 days based on the reported antibody disposition parameters estimated from data following intravenous administration. The bi-exponential decline of antibody concentrations in our dataset might be explained by the slow but long-lasting serum antibody production rate of the long-lived cells, which could be the rate-limiting step for antibody elimination, and would justify fixing the antibody disposition parameters in view of the flip-flop dynamics.

As previously observed with other biological processes, the present data suggest a more rapid time course of both production and disposition phases of humoral immune response in NHPs relative to humans where, for example, higher S-ELISA concentration values were reached earlier by the NHPs compared to humans following similar regimens (Sadoff et al. 2022b). In addition, allometric scaling described in humans (Davda et al., 2014) was applied to the disposition phase parameters in NHPs and improved the model fit. Data showed a well-maintained long-term durability which required $k_{eL}$ to be fixed to 0, indicating no waning of long-lived cells up to 20 weeks.

Inclusion of $k_{on}$ removed bias in the goodness-of-fit plots, adding weight to the hypothesis that secreted antibodies re-enter GC in affinity-dependent fashion and limit antigen access over time (Zhang et al., 2013). In addition, $k_{on}$ was included to describe faster decay after the

JPET Fast Forward. Published on August 3, 2023 as DOI: 10.1124/jpet.123.001591
This article has not been copyedited and formatted. The final version may differ from this version.

second peak observed in NHPs relative to humans by keeping $k_{eS}$ estimation consistent with the previously reported values (Nguyen et al., 2021).

According to the estimated model parameters, antibody production rate was greater for short-lived than long-lived cells, suggesting greater contribution of short-lived cells in driving peak response following Ad26.COV2.S vaccination. Immunization is believed to induce predominantly short-lived cell response mediated by the memory B cell pathway once memory B cells become relevant cell populations in the overall dynamic (Zhang et al., 2013; McNamara et al., 2020). This especially applied to the time course following the second dose of Ad26.COV2.S whereby a rapid and robust increase of antibody levels attributable to short-lived cells was observed. Following a second dose of Ad26.COV2.S, memory B cells are assumed to grow to a maximum value, consequently becoming a dominant route of short-lived cell production. By contrast, long-lived cells are assumed to be predominantly produced through GC (Zhang et al., 2013; McNamara et al., 2020). According to our model, antibody production mediated by long-lived cells were relevant for driving the peak post first dose and for driving the long-term time course of sustained antibody concentrations in all vaccination arms, in line with what was reported in vaccinated NHPs at day 315 (He et al. 2022).

The human mechanistic model (Dari et al., 2022) used a single-pathway equation (Balelli et al., 2020) for describing the B cell dynamics responsible for the production of short-lived and long-lived cells. Notably, the single-pathway model was not able to fit the binding antibody concentration time course in NHPs after injection of a dose of $1 \times 10^{11}$ vp, and showed biases in the goodness-of-fit plots. These observations led us to extend the operationalization of B cell compartment by considering the production of short-lived and long-lived cells as mediated directly through memory B cell ($M_1$) and GC ($M_2$) pathways (Zhang et al., 2013; McNamara et al., 2020), which better captured the follow-up antibody concentration increase after different regimens. The present data support the hypothesis regarding the relevance of a

JPET Fast Forward. Published on August 3, 2023 as DOI: 10.1124/jpet.123.001591
This article has not been copyedited and formatted. The final version may differ from this version.

dual pathway system for the production of long-lived and short-lived cells (Zhang et al., 2013; McNamara et al., 2020).

For the COVID-19 vaccines currently in use, antibodies targeting S protein are the strongest biomarkers of protection against SARS-CoV-2 infection (Goldblatt et al., 2022). In a prespecified correlate analysis of a phase 3 trial of a single-dose regimen of Ad26.COV2.S, increasing binding antibody concentrations at 4 weeks correlated with vaccine efficacy through 3 months post immunization (Fong et al., 2022). We recently used a mechanistic modeling-based approach in NHPs and demonstrated the relevance of SARS-CoV-2–binding antibody concentrations as a humoral biomarker of protection against viral replication in the lung and the nose of rhesus macaques vaccinated with single-dose Ad26.COV2.S (Roozendaal et al., 2021). The correlation between circulating antibody levels and protection appears to be better when assessing viral replication in the lung than in the nose. For instance, viral replication in the nose was found to be 50% higher than in the lung of NHPs (Roozendaal et al., 2021); consequently, the MIM of the binding antibodies was lower in the lung (1.85; 95% CI, 1.80 to 1.91 EU/mL $\log_{10}$) than in the nose (3.21; 95% CI, 2.85 to 3.81). According to the current mechanistic modeling simulations, antibody concentrations elicited by two-dose regimens through 20 weeks were higher than MIM associated with protection in the lung but lower than MIM associated with the protection in the nose. Two-dose regimens of Ad26.COV2.S might therefore be effective in conferring protection in the lower but less so in the upper airways of vaccinated NHPs. These results underline the strength of the proposed approach which helps in determining the durability of protection against SARS-CoV-2 infection via comparing the biomarker time course of different regimens with the MIM threshold.

Animal models, including monkey, have been widely used to evaluate the efficacy of vaccines as well as vaccination duration leading to the selection of immunization strategies in

JPET Fast Forward. Published on August 3, 2023 as DOI: 10.1124/jpet.123.001591
This article has not been copyedited and formatted. The final version may differ from this version.

humans (Qi and Qin (2022)). The current study enabled to evaluate different doses and regimens. However, animal models also have limitations, as they don't reproduce all key features after SARS-CoV-2 infection and the immune system is not identical when comparing between species (including humans and NHP). One avenue for future research could involve investigating translational applications of antibody-based thresholds associated with protection against viral replication in the lung of NHPs through the use of the same assays, enrollment of naïve subjects, and the use of similar structural models. Additional work could focus on conducting pooled analyses to quantify differences in the time course and mechanistic drivers of the humoral immune responses between humans and NHPs, including cellular immunity. On this regard, it would be relevant to further investigate the role of T cell responses in driving vaccine protection, or the durability thereof (McMahan et al., 2021). A thorough exploratory analysis should be performed to assess if the T cell contribution to protection is relevant for the vaccine under development. Furthermore, given the lack of humoral immune response data in NHPs induced by the second dose given with the interval >2 months, future studies should address the accuracy of model extrapolations as it pertains to the second dose administered beyond this time frame. Finally, given low number of NHPs and the homogeneity of the population, further data collection is needed to evaluate the influence of covariates (e.g., sex and age).

In conclusion, the six-compartment mechanistic model adequately described the time course of binding antibody concentrations and its associated variability elicited by vaccination with Ad26.COV2.S irrespective of dose level ($1 \times 10^{11}$ or $5 \times 10^{10}$ vp) or regimen (single-dose or homologous two-dose [$5 \times 10^{10}$ vp] given either 4 or 8 weeks apart). Deterministic simulations predicted that two-dose regimens (i.e., booster at 2, 4, 6, or 8 weeks) increase binding antibody concentrations relative to single-dose regimens in NHP, resulting in longer antibody persistence that might translate into longer duration of vaccine protection, as

JPET Fast Forward. Published on August 3, 2023 as DOI: 10.1124/jpet.123.001591
This article has not been copyedited and formatted. The final version may differ from this version.

observed in the clinical setting (Hardt et al. 2022). However, the optimal time to administer the booster dose is not translatable between NHP and human, because the kinetics of the immune response between NHP and humans are different. Given the difference in the immune system between NHP and human, the intent of the current mechanistic model was not to fully translate the time course of humoral response from NHP to human. Nevertheless, the adequacy of the mechanistic modeling approach to describe humoral immune response elicited by vaccination with Ad26.COV2.S in both humans (Dari et al., 2022) and NHPs suggests that immune system features described in humans and NHPs could be used to inform clinical studies. Although this research is applied to the Ad26.COV2.S vaccine, the acquired knowledge could be used to inform other vaccine platforms, different diseases, and also for vaccines in development for therapeutic use. The findings contribute data on the key biological components responsible for the observed time course of vaccine-induced humoral immunity in NHPs and are a step towards defining immune biomarkers of protection against SARS-CoV-2 that might translate across species.



## ACKNOWLEDGMENTS

The pooled NONMEM dataset preparation was provided by Frédéric Saad (Janssen Research & Development, LLC, Beerse, Belgium). Philippe Jacqmin assisted with the conceptual model development. Medical writing support was provided by Andreja Varjačić, PhD, of Eloquent Scientific Solutions, and was funded by Janssen Research & Development, LLC.

## DATA AVAILABILITY STATEMENT

The original data that support the findings of this analysis are included in a preprint article (and its supplementary information files) at https://www.researchsquare.com/article/rs-2207397/v1. The data sharing policy of the Sponsor is available at https://www.janssen.com/clinical-trials/transparency. As noted on this site, requests for

access to the study data can be submitted through Yale Open Data Access (YODA) Project site at http://yoda.yale.edu.

## AUTHOR CONTRIBUTIONS

Participated in research design: Solforosi L. and Roozendaal R.

Performed data analysis: Dari A., Boulton M. and Pérez Ruixo J.J.

Wrote or contributed to the writing of the manuscript: Dari A., Boulton M., Hoetelmans R.M.W., Pérez Ruixo J.J., Roozendaal R. and Solforosi L.

## REFERENCES:

Balelli I, Pasin C, Prague M, Crauste F, Effelterre TV, Bockstal V, Solforosi L, and Thiébaut R (2020) A model for establishment, maintenance and reactivation of the immune response after vaccination against Ebola virus. *J Theor Biol* **495:** 110254.

Bergstrand M, Hooker AC, Wallin JE, and Karlsson MO (2011) Prediction-corrected visual predictive checks for diagnosing nonlinear mixed-effects models. *AAPS J* **13:** 143-151.

Bonin CRB, Fernandes GC, Dos Santos RW, and Lobosco M (2018) A qualitatively validated mathematical-computational model of the immune response to the yellow fever vaccine. *BMC Immunol* **19:** 15.

Bos R, Rutten L, van der Lubbe JEM, Bakkers MJG, Hardenberg G, Wegmann F, Zuijdgeest D, de Wilde AH, Koornneef A, Verwilligen A, van Manen D, Kwaks T, Vogels R, Dalebout TJ, Myeni SK, Kikkert M, Snijder EJ, Li Z, Barouch DH, Vellinga J, Langedijk JPM, Zahn RC, Custers J, and Schuitemaker H (2020) Ad26 vector-based COVID-19 vaccine encoding a prefusion-stabilized SARS-CoV-2 Spike immunogen induces potent humoral and cellular immune responses. *NPJ Vaccines* **5:** 91.

Dari A, Boulton M, Neyens M, Le Gars M, Valenzuela B, Shukarev G, Cárdenas V, Ruiz-Guiñazú J, Sadoff J, Hoetelmans RMW, and Pérez Ruixo JJ (2022) Quantifying Antibody Persistence

After a Single Dose of COVID-19 Vaccine Ad26.COV2.S in Humans Using a Mechanistic Modeling and Simulation Approach. *Clin Pharmacol Ther*.

Davda JP, Dodds MG, Gibbs MA, Wisdom W, and Gibbs J (2014) A model-based meta-analysis of monoclonal antibody pharmacokinetics to guide optimal first-in-human study design. *MAbs* **6:** 1094-1102.

Dong JQ, Salinger DH, Endres CJ, Gibbs JP, Hsu CP, Stouch BJ, Hurh E, and Gibbs MA (2011) Quantitative prediction of human pharmacokinetics for monoclonal antibodies: retrospective analysis of monkey as a single species for first-in-human prediction. *Clin Pharmacokinet* **50:** 131-142.

Fong Y, McDermott AB, Benkeser D, Roels S, Stieh DJ, Vandebosch A, Le Gars M, Van Roey GA, Houchens CR, Martins K, Jayashankar L, Castellino F, Amoa-Awua O, Basappa M, Flach B, Lin BC, Moore C, Naisan M, Naqvi M, Narpala S, O'Connell S, Mueller A, Serebryannyy L, Castro M, Wang J, Petropoulos CJ, Luedtke A, Hyrien O, Lu Y, Yu C, Borate B, van der Laan LWP, Hejazi NS, Kenny A, Carone M, Wolfe DN, Sadoff J, Gray GE, Grinsztejn B, Goepfert PA, Little SJ, Paiva de Sousa L, Maboa R, Randhawa AK, Andrasik MP, Hendriks J, Truyers C, Struyf F, Schuitemaker H, Douoguih M, Kublin JG, Corey L, Neuzil KM, Carpp LN, Follmann D, Gilbert PB, Koup RA, and Donis RO (2022) Immune correlates analysis of the ENSEMBLE single Ad26.COV2.S dose vaccine efficacy clinical trial. *Nat Microbiol* **7:** 1996-2010.

Gilbert PB, Montefiori DC, McDermott AB, Fong Y, Benkeser D, Deng W, Zhou H, Houchens CR, Martins K, Jayashankar L, Castellino F, Flach B, Lin BC, O'Connell S, McDanal C, Eaton A, Sarzotti-Kelsoe M, Lu Y, Yu C, Borate B, van der Laan LWP, Hejazi NS, Huynh C, Miller J, El Sahly HM, Baden LR, Baron M, De La Cruz L, Gay C, Kalams S, Kelley CF, Andrasik MP, Kublin JG, Corey L, Neuzil KM, Carpp LN, Pajon R, Follmann D, Donis RO, and Koup RA (2022) Immune correlates analysis of the mRNA-1273 COVID-19 vaccine efficacy clinical trial. *Science* **375:** 43-50.

Goldblatt D, Alter G, Crotty S, and Plotkin SA (2022) Correlates of protection against SARS-CoV-2 infection and COVID-19 disease. *Immunol Rev* **310:** 6-26.

Gonçalves A, Maisonnasse P, Donati F, Albert M, Behillil S, Contreras V, Naninck T, Marlin R, Solas C, Pizzorno A, Lemaitre J. SARS-CoV-2 viral dynamics in non-human primates. PLoS computational biology. 2021 Mar 17;17(3):e1008785.

Gruell H, Vanshylla K, Weber T, Barnes CO, Kreer C, and Klein F (2022) Antibody-mediated neutralization of SARS-CoV-2. *Immunity* **55:** 925-944.

Hammarlund E, Thomas A, Amanna IJ, Holden LA, Slayden OD, Park B, Gao L, and Slifka MK (2017) Plasma cell survival in the absence of B cell memory. *Nat Commun* **8:** 1781.

Hardt K, Vandebosch A, Sadoff J, Le Gars M, Truyers C, Lowson D, Van Dromme I, Vingerhoets J, Kamphuis T, Scheper G, Ruiz-Guiñazú J, Faust SN, Spinner CD, Schuitemaker H, Van Hoof J, Douoguih M, and Struyf F (2022) Efficacy, safety, and immunogenicity of a booster regimen of Ad26.COV2.S vaccine against COVID-19 (ENSEMBLE2): results of a randomised, double-blind, placebo-controlled, phase 3 trial. *Lancet Infect Dis*.

He X, Chandrashekar A, Zahn R, Wegmann F, Yu J, Mercado NB, McMahan K, Martinot AJ, Piedra-Mora C, Beecy S, Ducat S, Chamanza R, Huber SR, van Heerden M, van der Fits L, Borducchi EN, Lifton M, Liu J, Nampanya F, Patel S, Peter L, Tostanoski LH, Pessaint L, Van Ry A, Finneyfrock B, Velasco J, Teow E, Brown R, Cook A, Andersen H, Lewis MG, Schuitemaker H, and Barouch DH (2021) Low-dose Ad26.COV2.S protection against SARS-CoV-2 challenge in rhesus macaques. *Cell* **184:** 3467-3473.e3411.

He X, Aid M, Chandrashekar A, Yu J, McMahan K, Wegmann F, Jacob-Dolan C, Maron JS, Atyeo C, Wan H, Sellers D. A homologous or variant booster vaccine after Ad26. COV2. S immunization enhances SARS-CoV-2–specific immune responses in rhesus macaques. Science Translational Medicine. 2022 Feb 22;14(638):eabm4996.

Inoue T, Moran I, Shinnakasu R, Phan TG, and Kurosaki T (2018) Generation of memory B cells and their reactivation. *Immunol Rev* **283:** 138-149.

Jacqmin P, Snoeck E, van Schaick EA, Gieschke R, Pillai P, Steimer JL, and Girard P (2007) Modelling response time profiles in the absence of drug concentrations: definition and performance evaluation of the K-PD model. *J Pharmacokinet Pharmacodyn* **34:** 57-85.

Koup RA, Donis RO, Gilbert PB, Li AW, Shah NA, and Houchens CR (2021) A government-led effort to identify correlates of protection for COVID-19 vaccines. *Nat Med* **27:** 1493-1494.

Machado BAS, Hodel KVS, Fonseca L, Pires VC, Mascarenhas LAB, da Silva Andrade LPC, Moret MA, and Badaró R (2022) The Importance of Vaccination in the Context of the COVID-19 Pandemic: A Brief Update Regarding the Use of Vaccines. *Vaccines (Basel)* **10**.

McMahan K, Yu J, Mercado NB, Loos C, Tostanoski LH, Chandrashekar A, Liu J, Peter L, Atyeo C, Zhu A, Bondzie EA, Dagotto G, Gebre MS, Jacob-Dolan C, Li Z, Nampanya F, Patel S, Pessaint L, Van Ry A, Blade K, Yalley-Ogunro J, Cabus M, Brown R, Cook A, Teow E, Andersen H, Lewis MG, Lauffenburger DA, Alter G, and Barouch DH (2021) Correlates of protection against SARS-CoV-2 in rhesus macaques. *Nature* **590:** 630-634.

McNamara HA, Idris AH, Sutton HJ, Vistein R, Flynn BJ, Cai Y, Wiehe K, Lyke KE, Chatterjee D, Kc N, Chakravarty S, Lee Sim BK, Hoffman SL, Bonsignori M, Seder RA, and Cockburn IA (2020) Antibody Feedback Limits the Expansion of B Cell Responses to Malaria Vaccination but Drives Diversification of the Humoral Response. *Cell Host Microbe* **28:** 572-585.e577.

Mercado NB, Zahn R, Wegmann F, Loos C, Chandrashekar A, Yu J, Liu J, Peter L, McMahan K, Tostanoski LH, He X, Martinez DR, Rutten L, Bos R, van Manen D, Vellinga J, Custers J, Langedijk JP, Kwaks T, Bakkers MJG, Zuijdgeest D, Rosendahl Huber SK, Atyeo C, Fischinger S, Burke JS, Feldman J, Hauser BM, Caradonna TM, Bondzie EA, Dagotto G, Gebre MS, Hoffman E, Jacob-Dolan C, Kirilova M, Li Z, Lin Z, Mahrokhian SH, Maxfield LF, Nampanya F, Nityanandam R, Nkolola JP, Patel S, Ventura JD, Verrington K, Wan H, Pessaint L, Van Ry A, Blade K, Strasbaugh A, Cabus M, Brown R, Cook A, Zouantchangadou S, Teow E, Andersen H, Lewis MG, Cai Y, Chen B, Schmidt AG, Reeves RK, Baric RS, Lauffenburger DA, Alter G,

Stoffels P, Mammen M, Van Hoof J, Schuitemaker H, and Barouch DH (2020) Single-shot Ad26 vaccine protects against SARS-CoV-2 in rhesus macaques. *Nature* **586:** 583-588.

Nguyen DC, Duan M, Ali M, Ley A, Sanz I, and Lee FE (2021) Plasma cell survival: The intrinsic drivers, migratory signals, and extrinsic regulators. *Immunol Rev* **303:** 138-153.

Nguyen TH, Mouksassi MS, Holford N, Al-Huniti N, Freedman I, Hooker AC, John J, Karlsson MO, Mould DR, Pérez Ruixo JJ, Plan EL, Savic R, van Hasselt JG, Weber B, Zhou C, Comets E, and Mentré F (2017) Model evaluation of continuous data pharmacometric models: metrics and graphics. *CPT Pharmacometrics Syst Pharmacol* **6:** 87-109.

Pasin C, Balelli I, Van Effelterre T, Bockstal V, Solforosi L, Prague M, Douoguih M, and Thiébaut R (2019) Dynamics of the humoral immune response to a prime-boost ebola vaccine: quantification and sources of variation. *J Virol* **93:** e00579-00519.

Qi F and Qin C (2022) Characteristics of animal models for COVID-19. *Animal Model Exp Med* **5:** 401-409.

Roozendaal R, Solforosi L, Stieh DJ, Serroyen J, Straetemans R, Dari A, Boulton M, Wegmann F, Rosendahl Huber SK, van der Lubbe JEM, Hendriks J, Le Gars M, Dekking L, Czapska-Casey DN, Guimera N, Janssen S, Tete S, Chandrashekar A, Mercado NB, Yu J, Koudstaal W, Perez-Ruixo JJ, Sadoff J, Barouch DH, Schuitemaker H, and Zahn R (2021) SARS-CoV-2 binding and neutralizing antibody levels after Ad26.COV2.S vaccination predict durable protection in rhesus macaques. *Nat Commun* **12:** 5877.

Sadoff J, Gray G, Vandebosch A, Cárdenas V, Shukarev G, Grinsztejn B, Goepfert PA, Truyers C, Fennema H, Spiessens B, Offergeld K, Scheper G, Taylor KL, Robb ML, Treanor J, Barouch DH, Stoddard J, Ryser MF, Marovich MA, Neuzil KM, Corey L, Cauwenberghs N, Tanner T, Hardt K, Ruiz-Guiñazú J, Le Gars M, Schuitemaker H, Van Hoof J, Struyf F, and Douoguih M (2021a) Safety and Efficacy of Single-Dose Ad26.COV2.S Vaccine against Covid-19. *N Engl J Med* **384:** 2187-2201.

Sadoff J, Gray G, Vandebosch A, Cárdenas V, Shukarev G, Grinsztejn B, Goepfert PA, Truyers C, Van Dromme I, Spiessens B, Vingerhoets J, Custers J, Scheper G, Robb ML, Treanor J, Ryser MF, Barouch DH, Swann E, Marovich MA, Neuzil KM, Corey L, Stoddard J, Hardt K, Ruiz-Guiñazú J, Le Gars M, Schuitemaker H, Van Hoof J, Struyf F, and Douoguih M (2022a) Final analysis of efficacy and safety of single-dose Ad26.COV2.S. *N Engl J Med* **386:** 847-860.

Sadoff J, Le Gars M, Brandenburg B, Cárdenas V, Shukarev G, Vaissiere N, Heerwegh D, Truyers C, de Groot AM, Jongeneelen M, Kaszas K, Tolboom J, Scheper G, Hendriks J, Ruiz-Guiñazú J, Struyf F, Van Hoof J, Douoguih M, and Schuitemaker H (2022b) Durable antibody responses elicited by 1 dose of Ad26.COV2.S and substantial increase after boosting: 2 randomized clinical trials. *Vaccine*.

Sadoff J, Le Gars M, Shukarev G, Heerwegh D, Truyers C, de Groot AM, Stoop J, Tete S, Van Damme W, Leroux-Roels I, Berghmans PJ, Kimmel M, Van Damme P, de Hoon J, Smith W, Stephenson KE, De Rosa SC, Cohen KW, McElrath MJ, Cormier E, Scheper G, Barouch DH, Hendriks J, Struyf F, Douoguih M, Van Hoof J, and Schuitemaker H (2021b) Interim results of a phase 1-2a trial of Ad26.COV2.S COVID-19 vaccine. *N Engl J Med* **384:** 1824-1835.

Savic RM and Karlsson MO (2009) Importance of shrinkage in empirical bayes estimates for diagnostics: problems and solutions. *AAPS J* **11:** 558-569.

Schley D, Tanaka RJ, Leungchavaphongse K, Shahrezaei V, Ward J, Grant C, Charleston B, and Rhodes CJ (2012) Modelling the influence of foot-and-mouth disease vaccine antigen stability and dose on the bovine immune response. *PLoS One* **7:** e30435.

Sherman AC, Desjardins M, and Baden LR (2022) Vaccine-induced severe acute respiratory syndrome coronavirus 2 antibody response and the path to accelerating development (determining a correlate of protection). *Clin Lab Med* **42:** 111-128.

Solforosi L, Costes L, Tolboom J, McMahan K, Anioke T, Hope D, Murdza T, Sciacca M, Bouffard E, Barrett J, Wu C, Hachmann N, Miller J, Yu J, He X, Jacob-Dolan C, Rosendahl Huber SK, Dekking L, Chamanza R, Choi Y, Feddes-de Boer K, Barouch D, Schuitemaker H, Zahn R, and

Wegmann F (2023) Booster immunization with Ad26.COV2.S or Omicron adapted vaccine enhanced immune responses and efficacy against SARS-CoV-2 Omicron in non-human primates. *Nat Commun* **14**(1): 1944.

Solforosi L, Kuipers H, Jongeneelen M, Rosendahl Huber SK, van der Lubbe JEM, Dekking L, Czapska-Casey DN, Izquierdo Gil A, Baert MRM, Drijver J, Vaneman J, van Huizen E, Choi Y, Vreugdenhil J, Kroos S, de Wilde AH, Kourkouta E, Custers J, van der Vlugt R, Veldman D, Huizingh J, Kaszas K, Dalebout TJ, Myeni SK, Kikkert M, Snijder EJ, Barouch DH, Böszörményi KP, Stammes MA, Kondova I, Verschoor EJ, Verstrepen BE, Koopman G, Mooij P, Bogers W, van Heerden M, Muchene L, Tolboom J, Roozendaal R, Brandenburg B, Schuitemaker H, Wegmann F, and Zahn RC (2021) Immunogenicity and efficacy of one and two doses of Ad26.COV2.S COVID vaccine in adult and aged NHP. *J Exp Med* **218**.

Wilson JN, Nokes DJ, Medley GF, and Shouval D (2007) Mathematical model of the antibody response to hepatitis B vaccines: implications for reduced schedules. *Vaccine* **25:** 3705-3712.

Zarnitsyna VI, Ellebedy AH, Davis C, Jacob J, Ahmed R, and Antia R (2015) Masking of antigenic epitopes by antibodies shapes the humoral immune response to influenza. *Philos Trans R Soc Lond B Biol Sci* **370**.

Zhang Y, Meyer-Hermann M, George LA, Figge MT, Khan M, Goodall M, Young SP, Reynolds A, Falciani F, Waisman A, Notley CA, Ehrenstein MR, Kosco-Vilbois M, and Toellner KM (2013) Germinal center B cells govern their own fate via antibody feedback. *J Exp Med* **210:** 457-464.

JPET Fast Forward. Published on August 3, 2023 as DOI: 10.1124/jpet.123.001591
This article has not been copyedited and formatted. The final version may differ from this version.

# FOOTNOTES

This project has been funded in whole or in part with federal funds from the Department of Health and Human Services, Administration for Strategic Preparedness and Response, Biomedical Advanced Research and Development Authority, under Other Transaction Agreement [HHSO100201700018C].

Anna Dari is the employee of Janssen Research and Development (a Johnson & Johnson company) and may hold stock in Johnson & Johnson. Laura Solforosi is the employee of Janssen Research and Development (a Johnson & Johnson company) and may hold stock in Johnson & Johnson. Ramon Roozendaal is the employee of Janssen Research and Development (a Johnson & Johnson company) and may hold stock in Johnson & Johnson. Richard M.W. Hoetelmans is the employee of Janssen Research and Development (a Johnson & Johnson company) and may hold stock in Johnson & Johnson. Juan José Pérez Ruixo is the employee of Janssen Research and Development (a Johnson & Johnson company) and may hold stock in Johnson & Johnson. Muriel Boulton is the employee of Janssen Research and Development (a Johnson & Johnson company) and may hold stock in Johnson & Johnson.

JPET Fast Forward. Published on August 3, 2023 as DOI: 10.1124/jpet.123.001591
This article has not been copyedited and formatted. The final version may differ from this version.

## FIGURE LEGENDS

**Fig. 1.** Schematic of the mechanistic model of humoral immune responses following multiple doses and regimens of Ad26.COV2.S. The model extends the mechanistic model previously used to describe the time course of antibody responses following single-dose Ad26.COV2.S in humans (Dari et al., 2022).

**Fig. 2.** The time course of binding antibody concentrations through 20 weeks post immunization with Ad26.COV2.S in all vaccination arms (n = 14 per arm). Dots and grey lines depict individual data. Coloured lines are geometric mean lines for the four active arms. Dotted blue line is the lower limit of quantification (LLOQ) based on assay quantification for human serum samples (50.3 $\log_{10}$ EU/mL; EU, ELISA unit) (A). Dose-normalized mean time course after single injection of Ad26.COV2.S stratified by dose (B).

**Fig. 3.** Goodness-of-fit plots of the mechanistic model for S-ELISA. (A) Observed concentrations vs. population-predicted and individual-predicted concentrations. (B) Conditional weighted residuals (CWRES) vs. population-predicted concentrations and vs. time. Red solid line is a LOWESS smoother. Blue and red dotted lines represent the $95^{th}$ and $99^{th}$ percentile of the CWRES distribution, respectively.

**Fig. 4.** Visual predictive check (VPC) of the time course of binding antibody concentrations and model predictions. Dots depict individual data. Red dotted lines are the geometric mean computed from the observations. Solid black lines are the simulated geometric means. Shaded areas represent the 80% prediction interval.

**Fig. 5.** Deterministic simulations of the time course of binding antibody concentrations (S-ELISA values on log10 scale) for interpolated regimens of Ad26.COV2.S ($5 \times 10^{10}$ vp): a single-dose regimen and homologous two-dose regimens given at an interval of 2, 4, 6, or 8 weeks.

JPET Fast Forward. Published on August 3, 2023 as DOI: 10.1124/jpet.123.001591
This article has not been copyedited and formatted. The final version may differ from this version.

**Table 1**. Design of the NHP mechanistic modeling study.

| **Treatment Group** | **Dose 1** | **Dose 2** | **N** |
|---|---|---|---|
| Ad26.COV2.S, Single Dose | $1 \times 10^{11}$ vp | - | 14 |
| Ad26.COV2.S, Single Dose | $5 \times 10^{10}$ vp | - | 14 |
| Ad26.COV2.S, Two Doses (Days 1 and 29; 4 wk) | $5 \times 10^{10}$ vp | $5 \times 10^{10}$ vp | 14 |
| Ad26.COV2.S, Two Doses (Days 1 and 57; 8 wk) | $5 \times 10^{10}$ vp | $5 \times 10^{10}$ vp | 14 |

N, number of animals; NHP, non-human primate; vp, viral particle.

**Table 2.** Median antibody concentrations (EU/mL $\log_{10}$) at the peak and at the end of the observation period (day 141) for all Ad26.COV2.S vaccination arms.

| **Time Point**<br><br>**Median (Q1, Q3),** | **Vaccination Arm** | | | |
|---|---|---|---|---|
| | Single Dose[a]<br><br>$1 \times 10^{11}$ (N = 14)[b] | Single Dose[a]<br><br>$5 \times 10^{10}$ (N = 14)[b] | Two Doses (4-wk interval)[a]<br><br>$5 \times 10^{10}$ (N = 14)[b] | Two Doses (8-wk interval)[a]<br><br>$5 \times 10^{10}$ (N = 14)[b] |
| Day 28; 4 wk (First peak) | 3.26 (3.16, 3.60) | 3.08 (2.81, 3.24) | 3.07 (3.03, 3.27) | 3.16 (3.03, 3.25) |
| Day 43; 6 wk (Second peak)[c] | – | – | 3.81 (3.63, 3.82) | – |
| Day 71; 10 wk (Second peak)[c] | – | – | – | 3.80 (3.70, 3.98) |
| Day 141 | 2.73 (2.45, 2.85) | 2.56 (2.39, 2.73) | 2.84 (2.62, 2.95) | 3.03 (2.81, 3.25) |

[a]Dose intensity expressed in viral particles. [b]At day 141, 7 NHPs were evaluated. [c]Second peak was computed at day 43 for the 4-week two-dose regimen and at day 71 for the 8-week two-dose regimen. NHP, non-human primate.

JPET Fast Forward. Published on August 3, 2023 as DOI: 10.1124/jpet.123.001591
This article has not been copyedited and formatted. The final version may differ from this version.

**Table 3.** Parameter estimates and 95% CI from the model fit.

| Parameter | Unit | Estimate | 95% CI |
|---|---|---|---|
| Ad26 antigen decay, $k_{Ag}$ | $day^{-1}$ | 0.065 | Fixed |
| S protein–Ab complex formation, $k_{on}$ | $day^{-1}$/(EU/mL) | $1.15 \cdot 10^{-4}$ | $0.92 \cdot 10^{-4}$ to $1.38 \cdot 10^{-4}$ |
| Mem B production rate (antigen dependent, $k_{pAg}$) | Cells/vp/day | 1 | Fixed following reparameterization of the model (Dari et al., 2022) |
| Mem B production rate (antigen independent, $k_{pM}$) | $day^{-1}$ | 0.183 | 0.152 to 0.214 |
| B cell decay in $M_1$ and $M_2$, $k_{eM_1}$ and $k_{eM_2}$ | $year^{-1}$ | 0 | Fixed due to short follow-up |
| Maximum B cell produced ($N_1$) | Cells | $49.6 \cdot 10^4$ | $45.4 \cdot 10^4$ to $53.8 \cdot 10^4$ |
| S production rate – B-cell dependent, $k_{pS}$ | $day^{-1}$/vp | $0.5 \cdot 10^{-5}$ | Fixed based on sensitivity analysis |
| S elimination half-life, $k_{eS}$ | $day^{-1}$ | 0.31 | 0.21 to 0.40 |
| L production rate – B-cell dependent, $k_{pL}$ | $day^{-1}$/vp | $0.5 \cdot 10^{-5}$ | Fixed based on sensitivity analysis |
| L elimination half-life, $k_{eL}$ | $year^{-1}$ | 0 | Fixed |
| Ab production rate by S, $k_{AbS}$ | $day^{-1} \cdot$ (EU/mL)/Cells | 2.37 | 1.39 to 3.35 |

JPET Fast Forward. Published on August 3, 2023 as DOI: 10.1124/jpet.123.001591
This article has not been copyedited and formatted. The final version may differ from this version.

| **Parameter** | **Unit** | **Estimate** | **95% CI** |
|---|---|---|---|
| Ab production rate by L, $k_{AbL}$ | $day^{-1}$ · (EU/mL)/Cells | 0.582 | 0.437 to 0.727 |
| Central-to-peripheral rate, $k_{AbP}$ | $day^{-1}$ | 0.41 | Fixed |
| Peripheral-to-central rate, $k_{PAb}$ | $day^{-1}$ | 0.54 | Fixed |
| Ab decay rate, $k_{eAb}$ | $day^{-1}$ | 0.11 | Fixed |
| **Inter-individual variability** | | **CV[a] (%)** | **Shrinkage[b] (%)** |
| On $k_{AbL}$ | | 116.3 | 2.17 |
| On $k_{AbS}$ | | 191.4 | 12.2 |
| On $k_{pM}$ | | 53.5 | 16.7 |
| On $k_{eS}$ | | 118.0 | 18.5 |
| Proportional error[c] | | 9.02 | 17.6 |

[a]CV% derived as sqrt(exp(ω)-1)*100. [b]Shrinkage derived as $1 - SD(\eta_i)/sqrt(\omega^2)$. [c]Proportional error refers to original values (i.e., additive error on log-transformed values). Ab, antibody; Ad26, adenovirus serotype 26; CI, confidence interval; CV, coefficient of variation; S, spike; S-ELISA, spike protein–enzyme-linked immunosorbent assay; vp, viral particle.

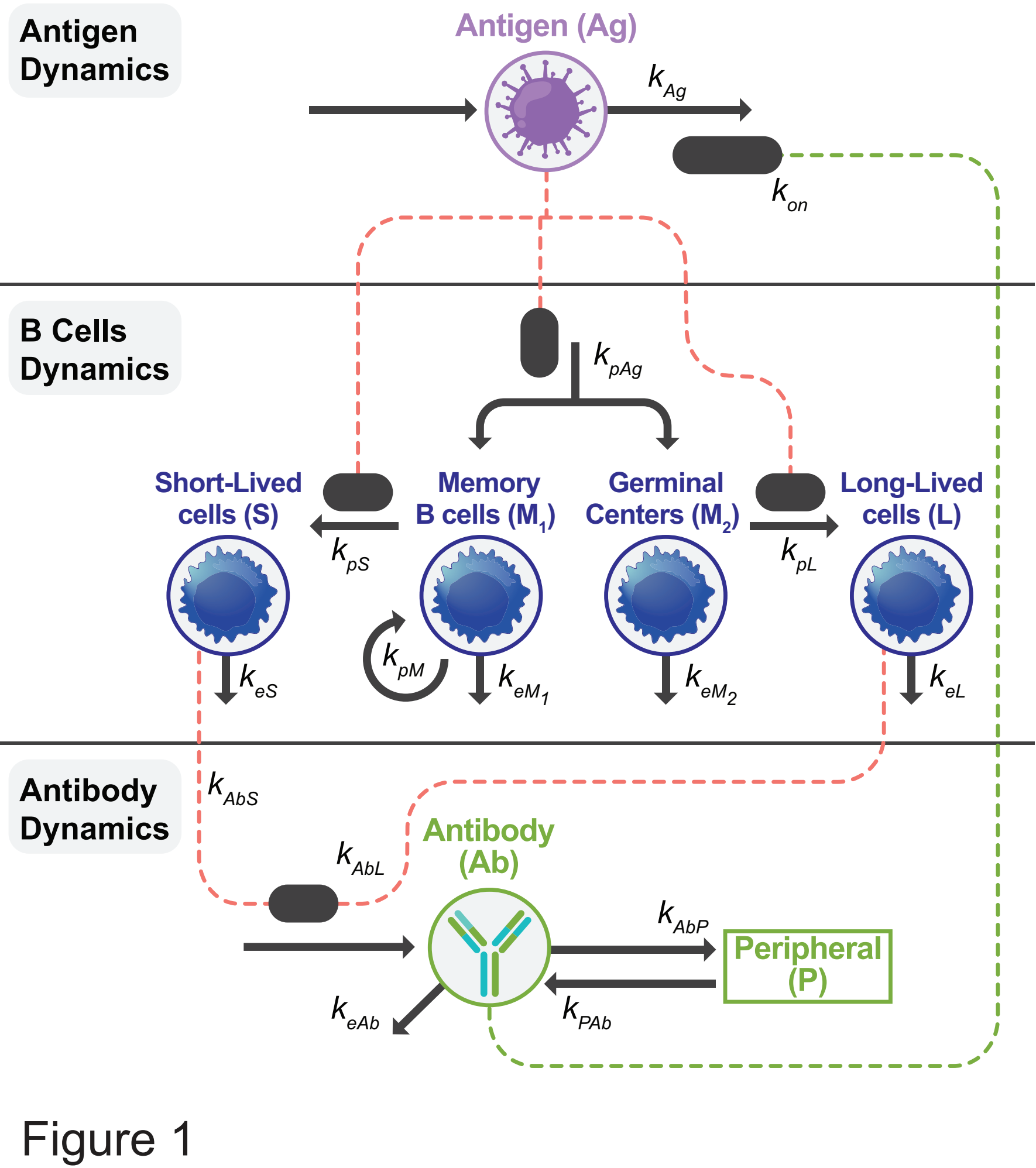
Antigen Dynamics
Antigen (Ag)
$k_{Ag}$
$k_{on}$
B Cells Dynamics
$k_{pAg}$
Short-Lived cells (S)
Memory B cells ($M_1$)
Germinal Centers ($M_2$)
Long-Lived cells (L)
$k_{pS}$
$k_{pL}$
$k_{pM}$
$k_{eS}$
$k_{eM_1}$
$k_{eM_2}$
$k_{eL}$
Antibody Dynamics
$k_{AbS}$
$k_{AbL}$
Antibody (Ab)
$k_{AbP}$
Peripheral (P)
$k_{eAb}$
$k_{PAb}$

Figure 1

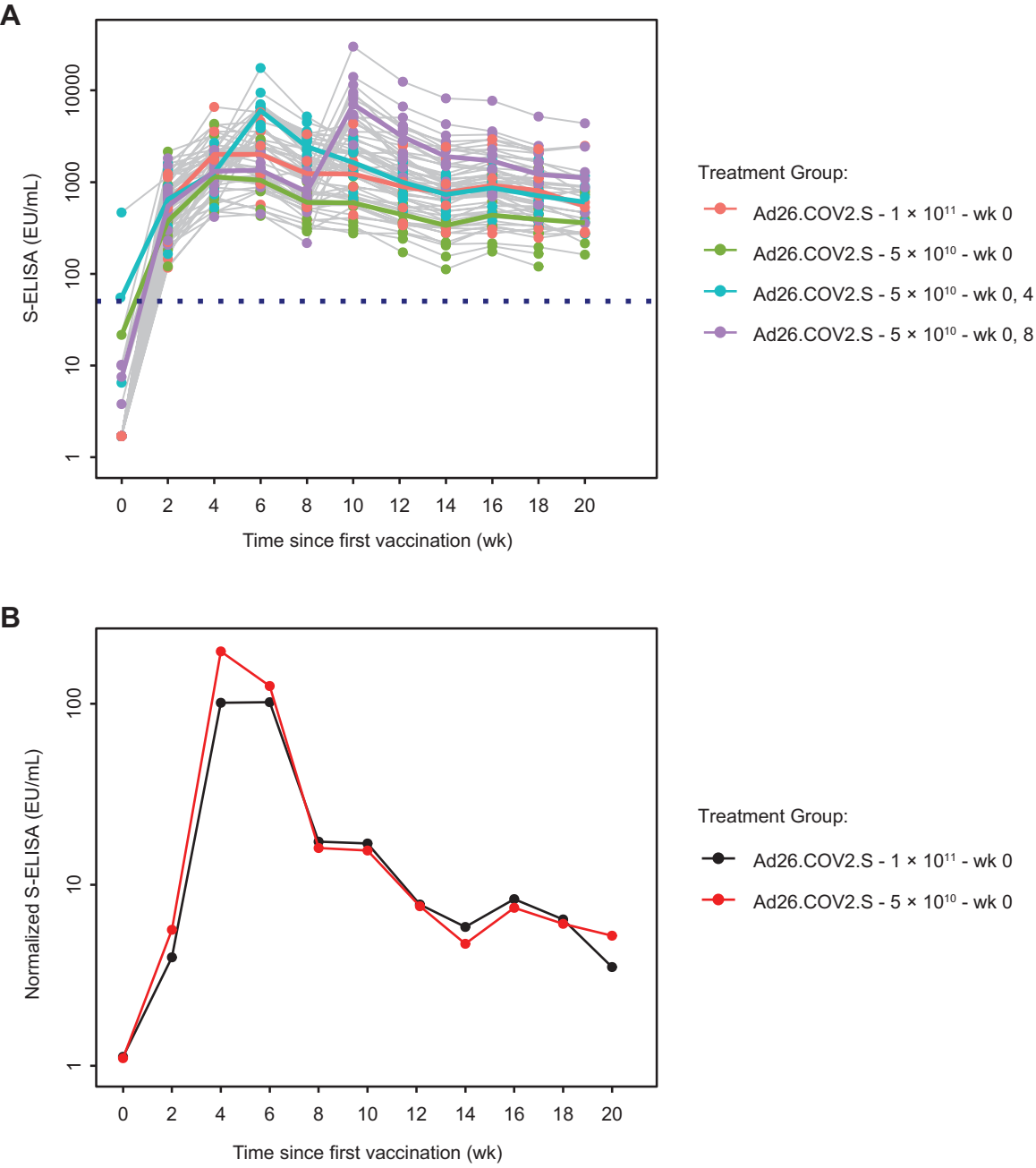
A
S-ELISA (EU/mL)
1
10
100
1000
10000
0
2
4
6
8
10
12
14
16
18
20
Time since first vaccination (wk)
Treatment Group:
Ad26.COV2.S - 1 × 10^11 - wk 0
Ad26.COV2.S - 5 × 10^10 - wk 0
Ad26.COV2.S - 5 × 10^10 - wk 0, 4
Ad26.COV2.S - 5 × 10^10 - wk 0, 8
B
Normalized S-ELISA (EU/mL)
1
10
100
0
2
4
6
8
10
12
14
16
18
20
Time since first vaccination (wk)
Treatment Group:
Ad26.COV2.S - 1 × 10^11 - wk 0
Ad26.COV2.S - 5 × 10^10 - wk 0

Figure 2

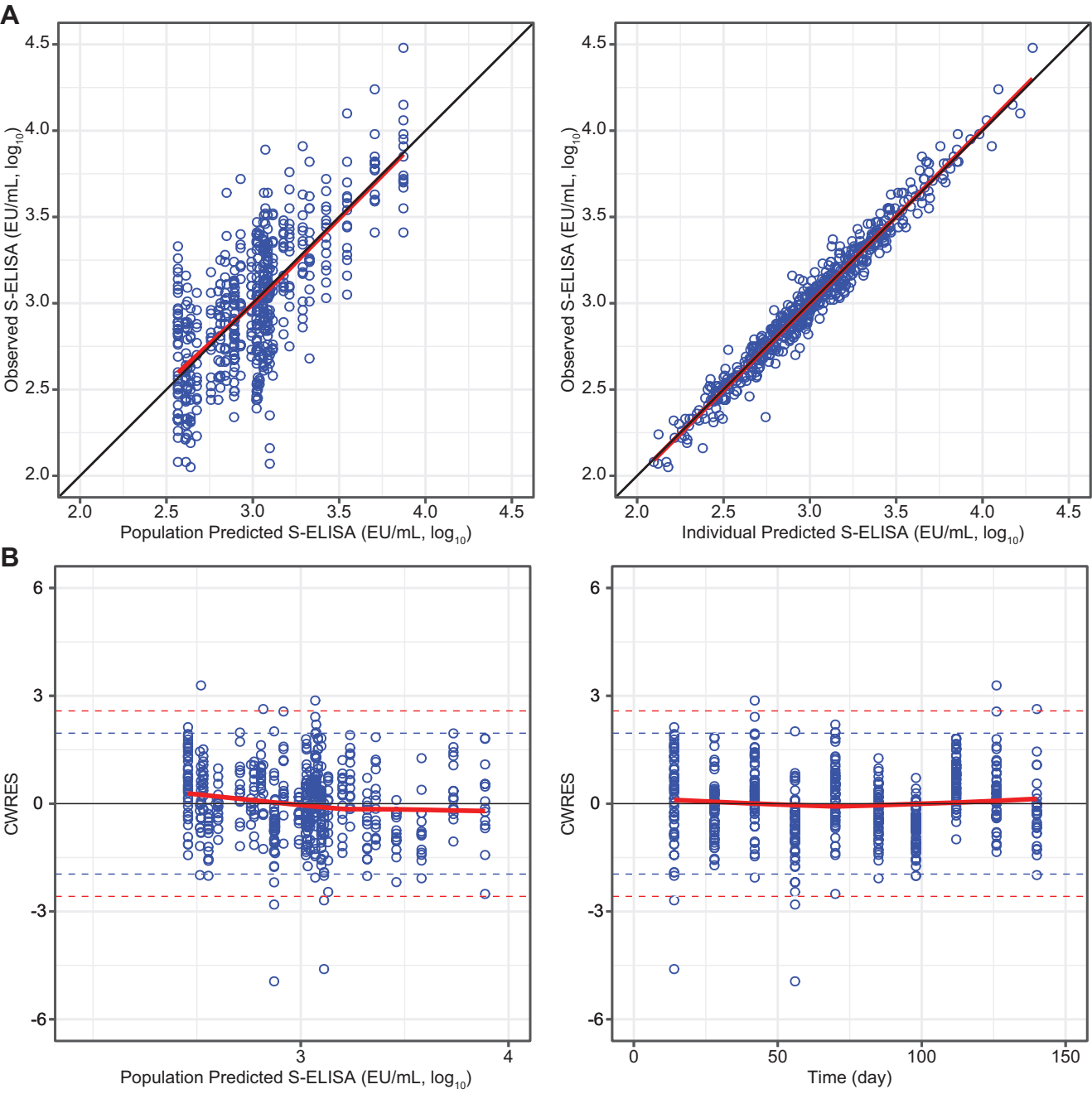
A
Observed S-ELISA (EU/mL, log10)
Population Predicted S-ELISA (EU/mL, log10)
Individual Predicted S-ELISA (EU/mL, log10)
B
CWRES
Population Predicted S-ELISA (EU/mL, log10)
Time (day)

Figure 3

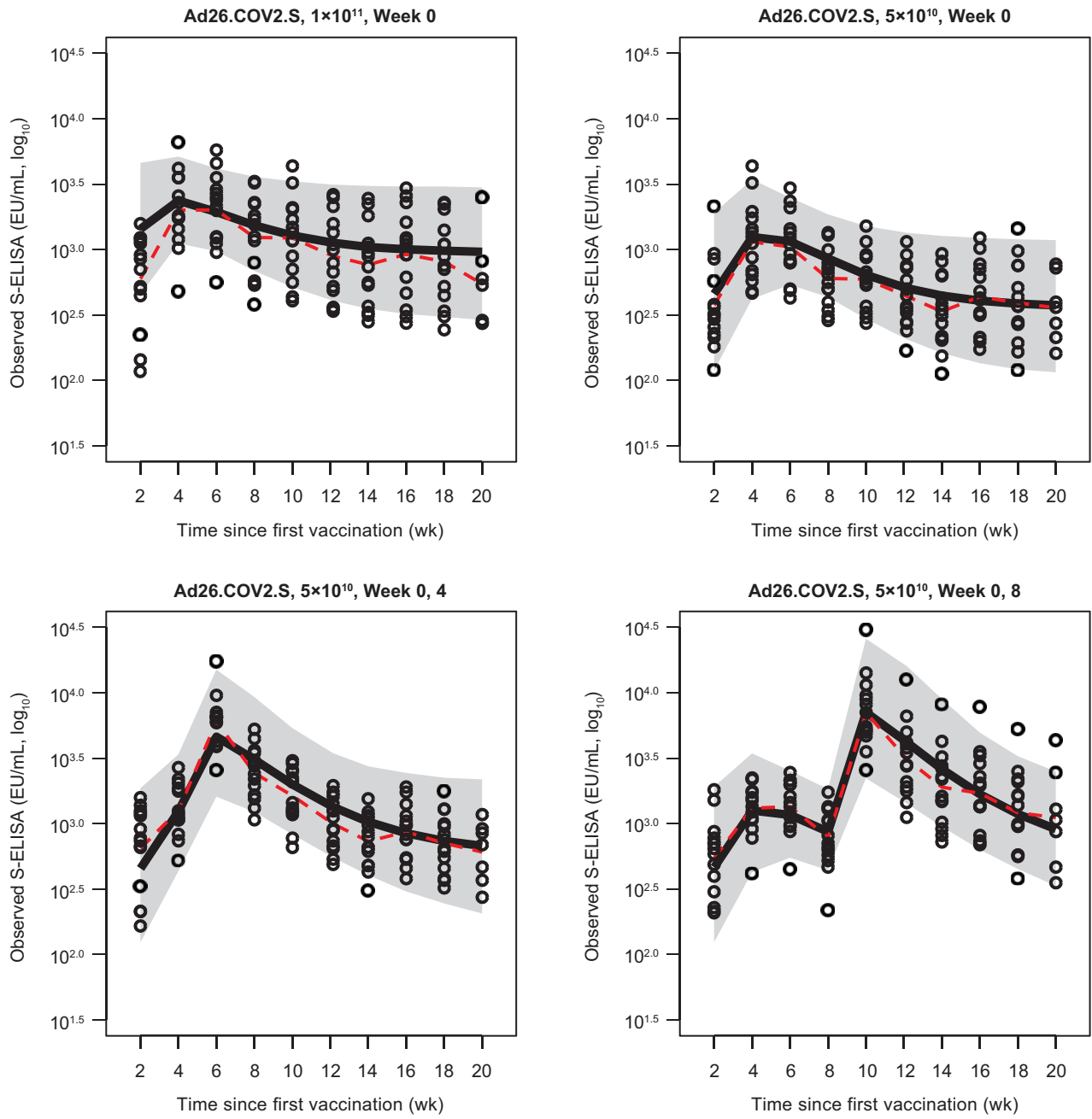
Ad26.COV2.S, 1×10¹¹, Week 0
Ad26.COV2.S, 5×10¹⁰, Week 0
Ad26.COV2.S, 5×10¹⁰, Week 0, 4
Ad26.COV2.S, 5×10¹⁰, Week 0, 8
Observed S-ELISA (EU/mL, log10)
10^4.5
10^4.0
10^3.5
10^3.0
10^2.5
10^2.0
10^1.5
2 4 6 8 10 12 14 16 18 20
Time since first vaccination (wk)

Figure 4

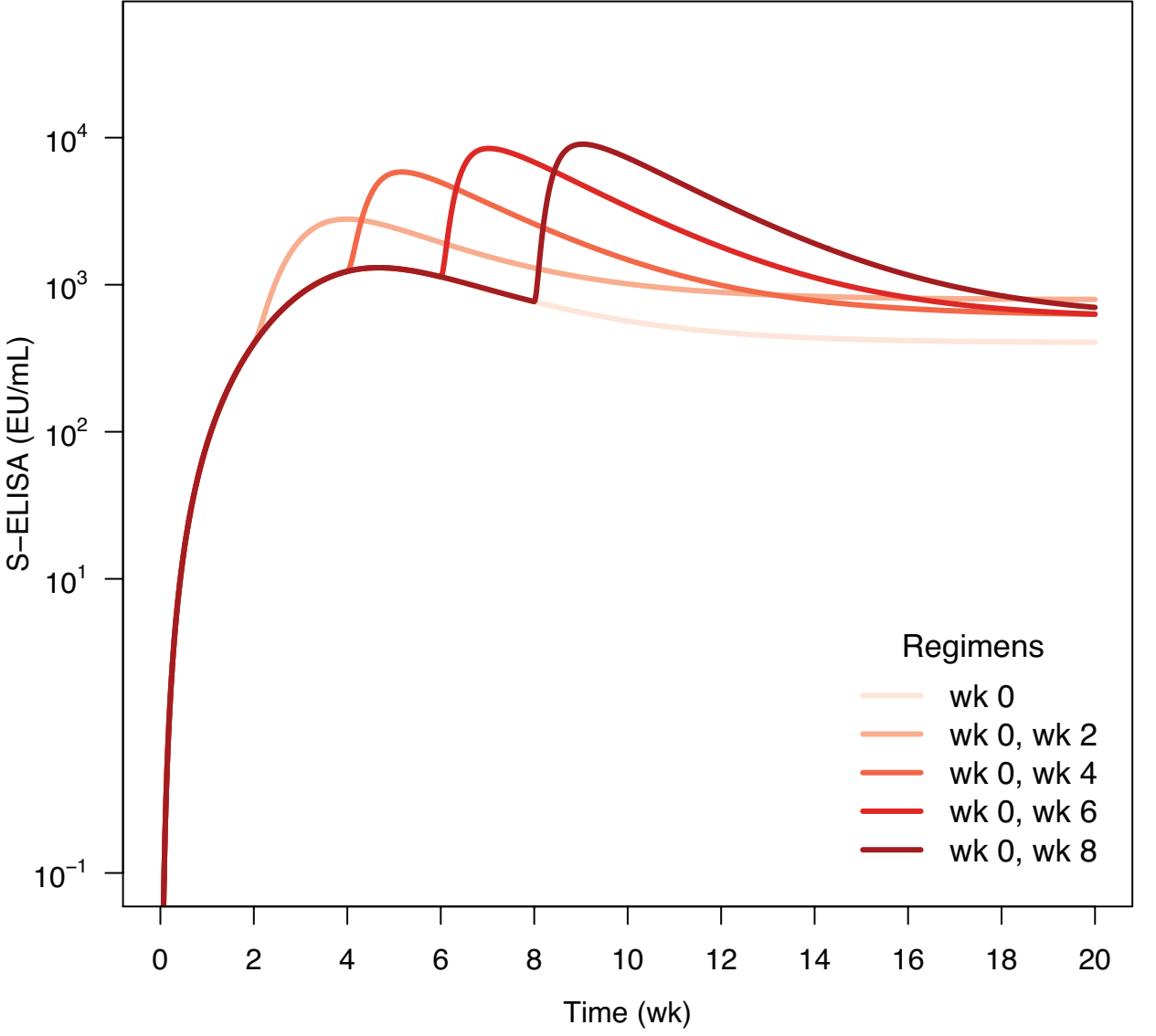
S−ELISA (EU/mL)
$10^4$
$10^3$
$10^2$
$10^1$
$10^{-1}$
0
2
4
6
8
10
12
14
16
18
20
Time (wk)
Regimens
wk 0
wk 0, wk 2
wk 0, wk 4
wk 0, wk 6
wk 0, wk 8

Figure 5